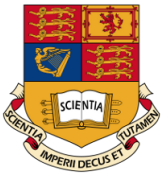

Improving Time Resolution of BCM1F

DESY Summer Student Programme, 2012

Pueh Leng Tan

Imperial College London, United Kingdom

Supervisors
Wolfgang Lohmann, Elena Castro

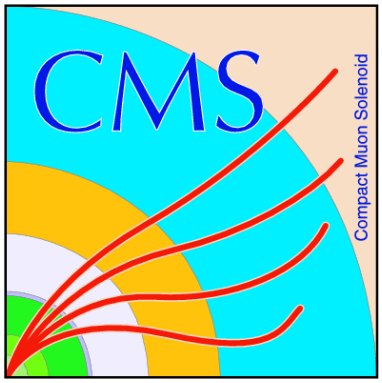

August 31, 2012

Abstract

Located inside the CMS pixel detector volume, the Fast Beam Conditions Monitor, BCM1F, is designed for the fast flux monitoring for both beam halo and collision product. Such monitoring is necessary to protect the CMS sub-detectors from unnecessary radiation damage. With its current time resolution, the BCM1F is unable to clearly resolve the signals from the beam halo which arrive 12 ns before the signals from the collision products. An improvement in time resolution of BCM1F can be achieved by upgrading the existing fixed threshold discriminators to constant fraction discriminators. Comparing various discriminators yield promising results, with both constant fraction discriminators (v812, CFD950) showing clear improvements in time resolution. Considering signals with input amplitudes of approximately 50mV, v812 improved the time resolution by slightly more than a factor of 3 while CFD950 improved time resolution by approximately a factor of 2. However, compared to v812, CFD950 has a shorter dead time of $(11.0 \pm 0.3)ns$ for input pulses with widths less than 50ns while the of the dead time of v812 is yet to be understood thoroughly.

Contents

1 Introduction

1.1 LHC and CMS

The Large Hadron Collider (LHC) at CERN is a particle accelerator capable of colliding protons up to 7 TeV per beam [1]. Built in a circular tunnel 27km in circumference, the LHC houses 4 main experiments designed to shed light on fundamental open questions in physics. The Compact Muon Solenoid (CMS) experiment is one of the experiments, and its main goals include searching for the Higgs boson and looking for evidence of physics beyond the standard model [2].

1.2 BCM1F

With proton intensities of more than 1e14 particles per beam [1] in the LHC, the beams generate a flux of halo particles near the beam-pipe as they interact with the residual particles in the vacuum, subjecting the CMS detector to high levels of radiation. Although the most innermost detectors are designed to withstand such levels of irradiation, the front-end electronics are still vulnerable to ionisation from short term beam losses. Such effects can also saturate the detectors, impeding data collection [3]. There is hence a need for beam tuning and protection of the CMS detector from adverse beam conditions. The Fast Beam Conditions Monitor, BCM1F, located inside the CMS pixel detector volume close to the beam-pipe uses sCVD diamond sensors to monitor the fast flux due to both beam halo and collision products. Although BCM1F is able to resolve the bunch crossings from which the collision products originate, it is unable to resolve particles from the beam halo arriving 12ns before the collision products. Information on the beam halo is crucial for flagging problematic beam conditions (such as from local vacuum problems) and post-mortem analysis after beam abort, hence, there is a need to improve the time resolution of the BCM1F detectors. This can be achieved by upgrading the discriminators that discriminate the pulses from the sCVD diamond sensors.

1.3 Discriminators

1.3.1 Rationale of upgrading discriminators

There are 2 main types of discriminators - fixed threshold discriminator (FTD) and constant fraction discriminator (CFD). The former produces an output pulse once the input signal has risen beyond a designated threshold while the latter produces an output pulse once the input has risen beyond a certain fraction of the full input signal.

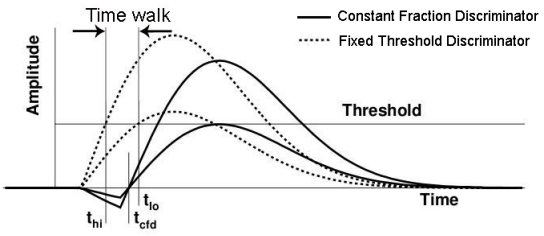

Figure 1: Constant fraction discriminator triggers on the zero-crossing, hence reducing the time walk as compared to the triggering mechanism that the fixed threshold discriminator employs [4].

As seen in figure 1, input signals of different amplitudes will trigger the fixed threshold discriminator at different times even though they arrive at the same time at the discriminator. This is known as 'time walk' and it compromises on the time resolution of the BCM1F monitoring system. On the other hand, the constant fraction discriminator processes the input signal and is triggered at the point in which the processed signal crosses the time axis, hence reducing the time walk significantly [5].

1.3.2 Principle of operation of CFD

The constant fraction discriminator works by adding a delayed and inverted copy of the input signal, shown in blue in figure 2, to the original copy, shown in black in figure 2. The discriminator is triggered at the zero-crossing of the resulting signal, shown in red in figure 2, and gives a square output pulse.

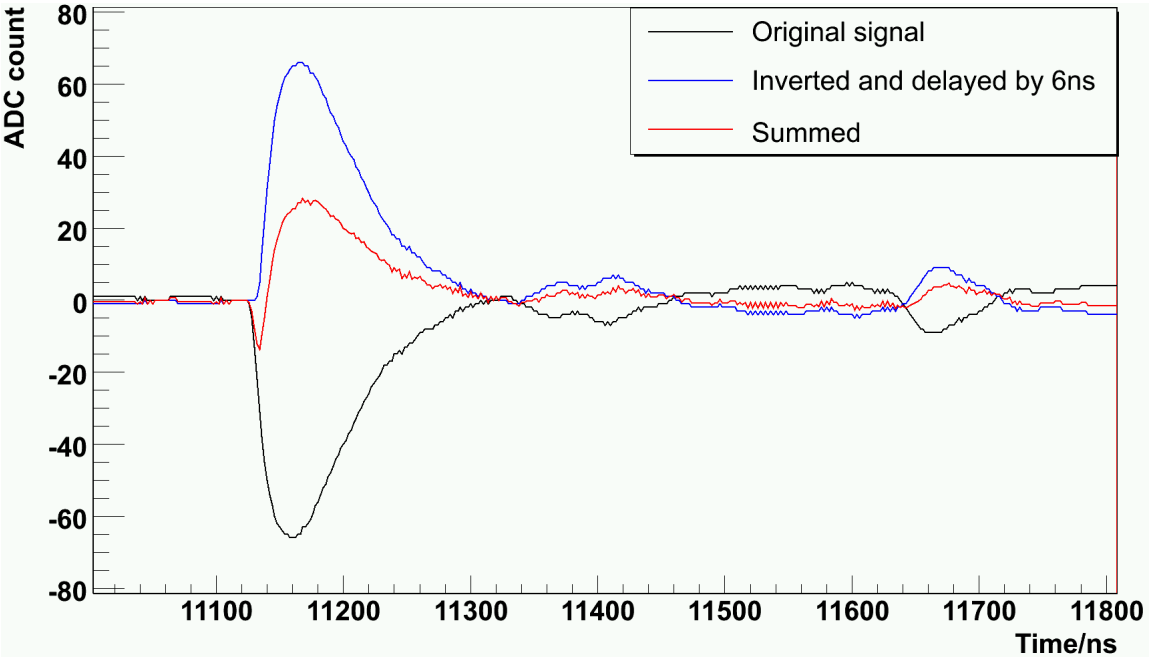

Figure 2: This plot was obtained by applying the working principles of the constant fraction discriminator to the signals sampled by the ADC.

Considering the rising edge of the signal with rise-time t_r and amplitude V_0,

$$V(t) = \frac{t}{t_r} V_0 \; for \; t \leq t_r$$

$$V(t) = V_0 \; for \; t > t_r$$

Delaying the signal by t_d gives $V(t) = \frac{t-t_d}{t_r} V_0$ and triggering on the zero-crossing implies $fV_0 = \frac{t-t_d}{t_r} V_0$ where f is the constant fraction by which the original signal was attenuated. As such, the point of trigger is independent on the amplitude of the signal [5]. For proper operation of the constant fraction discriminator, the internal delay should be greater than zero but less than the rise time of the input signal [4].

2 Methodology

2.1 Characterisation of discriminators

2 constant fraction discriminators were investigated (CAEN v812, PSI CFD 950), and a fixed threshold discriminator was used as a benchmark (CAEN v258B). The discriminators were characterised before their time resolutions were measured. Characterisation refers to the measurement of the discriminators' intrinsic properties, such as offset, pulse width, walk and dead time. The discriminators were controlled via VME. THey were placed in a VME crate and connected to the PC via a VME to PCI bridge. The code for the module was written in C++.

2.2 Measurement of double-hit resolution

2.2.1 Variation of dead time of constant fraction discriminators with pulse width(CFD950, v812)

Pseudo dead time refers to the minimal time interval between the rising edge of two consecutive input pulses for the discriminator to resolve the two input pulses. Dead time is obtained by subtracting the pulse width from the Pseudo dead time.

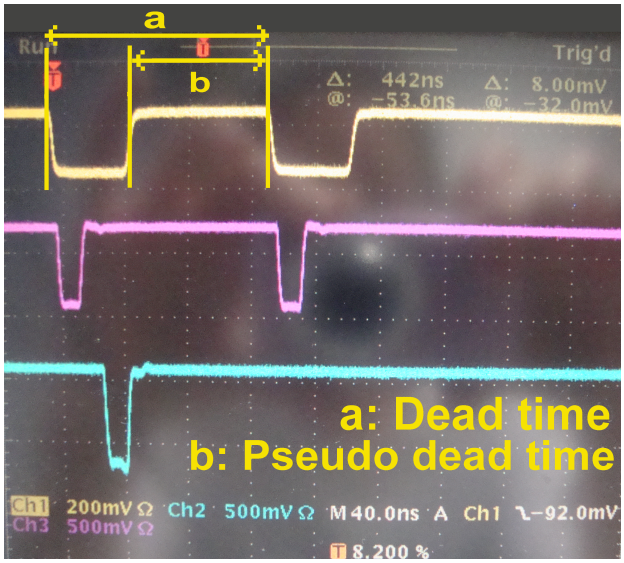

Figure 3: Definitions of dead time and pseudo dead time.

Input signal (inverted square pulses)
Rise time = 2.5 ns (smallest possible by function generator)
Time delay = 11ns to 193ns for CFD950, 10ns to 161ns for v812
Period = 100 μs
Width = 4ns to 1000ns for CFD950, 21ns to 170ns for v812
Amplitude = 200mV

Table 1: Parameters of input signal used to characterise dead time of the constant fraction discriminators.

Two identical periodic inverted square pulses were generated independently with a time delay between them. The time delay ($\sim 100ns$) was considerably shorter than the period of the pulses ($100\mu s$). The pulses were then mixed in a fan-in fan-out to generate the period burst of two square pulses. The time delay between the two square pulses within a burst was adjusted until two clear discriminator outputs were observed on the oscilloscope. The dead time of the discriminators were measured using the oscilloscope for various input pulse widths.

2.3 Measurement of time resolution

2.3.1 Sinusoidal modulations

It was not possible to generate signals of a fixed baseline but with changing amplitudes. To overcome this technical constraint, an input signal was modulated with a sinusoidal signal at a much lower frequency to simulate an input with changing amplitude.

Input signal (pulsed)	Modulating signal (sinusoidal)
Rise time = 28 ns	Frequency = 100 Hz
Amplitude = 50 mV, 100 mV, 200 mV, 300 mV	Amplitude = 10 mV, 20 mV
Generated by PM 5786B	Generated by Tektronix AFG 3252

Table 2: Parameters of input signal to discriminators and modulating sinusoidal signal to simulate input signals with fluctuating amplitudes.

2.3.2 Experimental set-up

The experimental set-up is described in figure 4. The input pulse and sinusoidal modulation are generated and attenuated independently before being mixed in a fan-in fan-out. Identical copies are sent to each of the discriminators, with the discriminator output fed to the TDC. The TDC is triggered at start using the clock output of the input pulse generator (PM 5786B) which has been translated to the correct standard using a series of translators (CAEN N89, v538). The TDC gives a text file and root file which were processed using ROOT to create histograms of the arrival times of the various discriminator outputs. The histograms of discriminator output arrival times were then fitted in ROOT to find the underlying distribution. The RMS of the histograms were taken to be the time resolution of the discriminators.

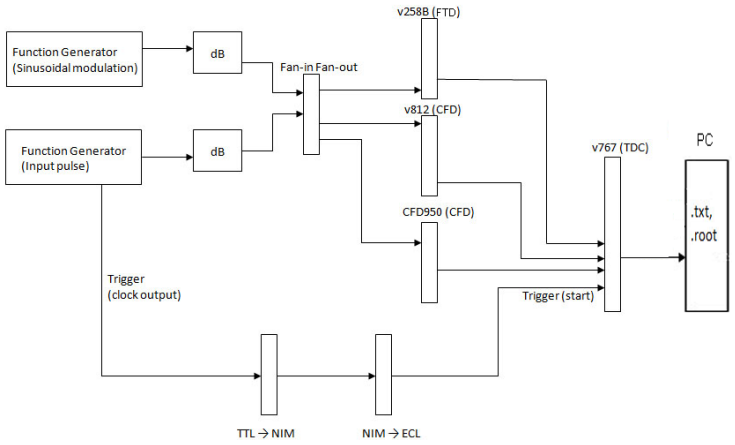

Figure 4: Schematic of the set-up for measuring the time resolution of the discriminators.

Keeping the code threshold at -20mV and modulating amplitude of 10mV, the time resolution of the 3 discriminators were measured with varying input amplitude (50mV to 300mV). The same measurement was repeated but with modulating amplitude of 20mV. For the measurement with 10mV modulating amplitude, the arrival time histograms were summed over the various input amplitudes for each discriminator respectively. The root mean square (RMS) of the histograms give an indication of the resolution of the discriminators over a range of input signal amplitudes.

3 Results and Discussions

3.1 Dead time of constant fraction discriminators (CFD950, v812)

3.1.1 PSI CFD950

With $R^2 = 0.9937$, the relationship between the pseudo dead time of CFD950 and input pulse width can be described by a linear relationship with gradient of 1.1044 and y-intercept of 11.837. The relationship between the dead time and pulse width, however, is a step function. It has an average value of $(11.0 \pm 0.3)ns$ for pulse width less than 50 ns and ignoring the anomalous point at pulse widths of 200ns and 300ns, the average rises to an average of $(29.7 \pm 0.9)ns$ for pulse widths between 75 ns and 350 ns. The standard deviation was taken as the error of the average dead time. While the discontinuity of the dead time of CFD950 at pulse width between 50 and 75 ns should be taken note of, this discontinuity will not pose a problem as long as the rise time and width of a signal stays within a regime in which the dead time of CFD950 remains approximately constant.

3.1.2 CAEN v812

There are 3 regimes in the plot for v812. The curve starts off with a steep negative slope for input pulses with widths between 21ns and 22ns, followed by a relatively flat region for input pulses with widths from 25 to 125ns. The pseudo dead time then rises with increasing pulse width for signals with widths between 130ns and 170ns. These 3 regimes are also reflected in the plot of dead time against input pulse width but further investigations should be carried out for a thorough understanding of the relationship between the dead

time and the pulse width of v812.

It is imperative to note that the discriminator dead times are sensitive towards the nature of the input pulse. Therefore, the discriminators should be subjected to more realistic test pulses, such as pulses with rise time, pulse width and pulse form similar to the actual signals from the BCM1F sensors.

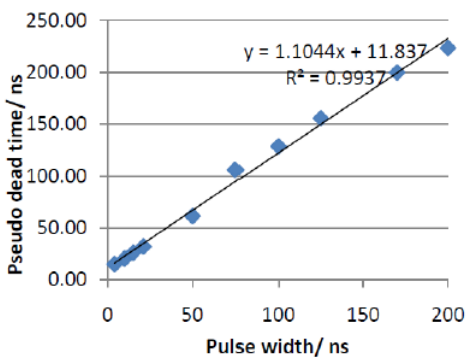

(a) Linear relationship between pseudo dead time and input pulse width obtained for CFD950.

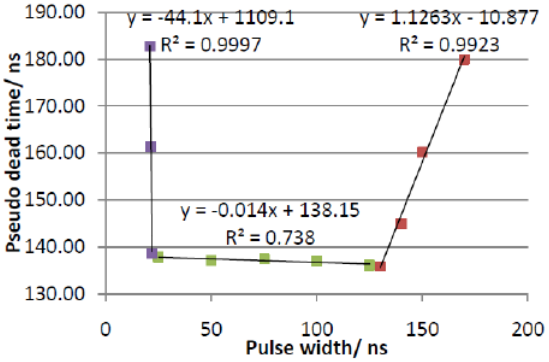

(b) Relationship between pseudo dead time of v812 and input pulse width comprised of 3 linear segments.

Figure 5: Dead time and Pseudo dead time of v812 and CFD950.

3.2 Measurement of time resolution

3.2.1 Sinusoidal modulation

The absolute arrival times of the discriminator outputs at the TDC are not relevant in this analysis and the discriminators were artificially delayed using wires so that the histograms are spaced out for the ease of viewing and analysis. TDC has resolution of 0.7ns and the histograms were binned with 1ns bins. Histograms of discriminator output arrival times were fitted the best with Gaussian distributions. This is expected as each discriminator output arrival time is randomly drawn from its underlying distribution. By central limit theorem [central limit theorem], the overall arrival times of each discriminator will be approximately normally distributed given that the sample size is sufficiently large (each histogram has around 4000 entries).

Comparing the χ^2 and the number of degrees of freedom of the fits, the Gaussian fit is more suitable for the constant fraction discriminators (CFD950, v812) than for the fixed threshold discriminator (v258B). The goodness of the fit may also be improved by accumulating more statistics.

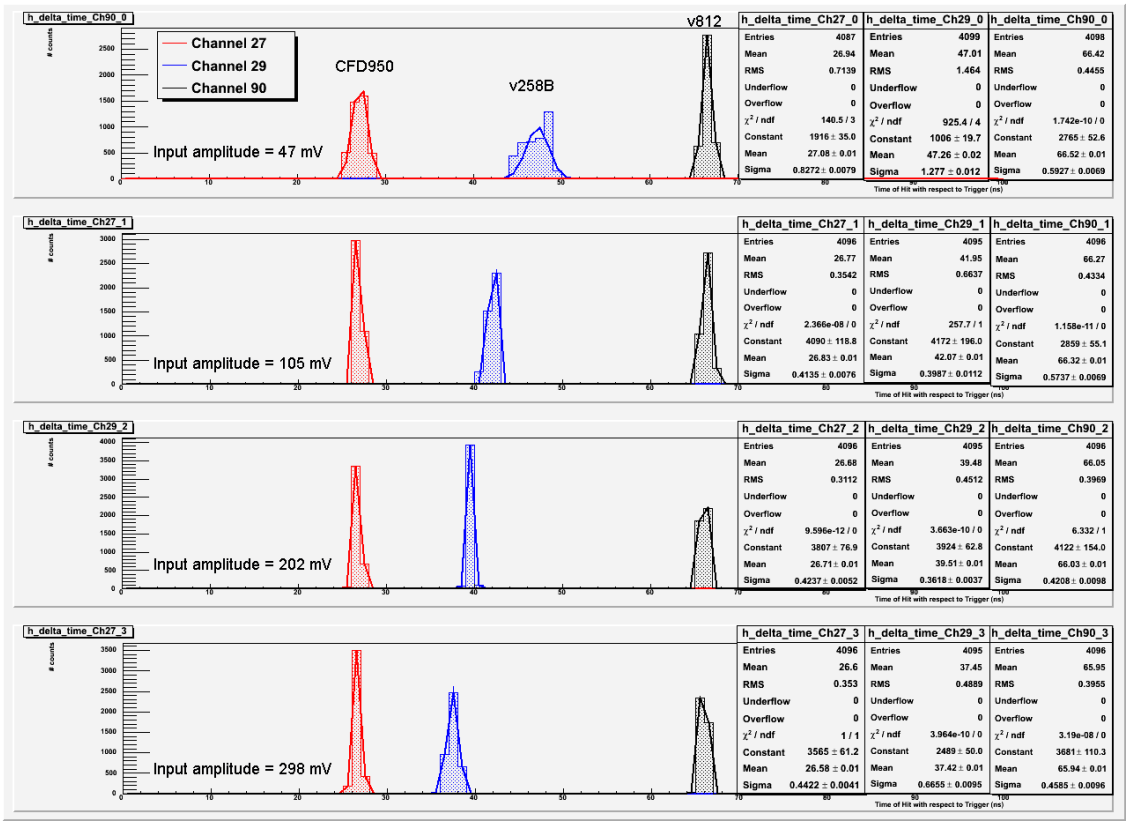

Figure 6: The time resolution of the fixed threshold discriminator (v258B) and constant fraction discriminators (v812, CFD95) for input signals of different amplitudes with sinusoidal modulation amplitude of 10mV.

The RMS of the histograms give an indication of the time resolutions of the discriminators but this includes the contribution from the TDC's time resolution as well. Such systematic errors can be reduced by taking the ratio of the discriminator resolutions instead of the absolute value.

Input amplitude/ mV	$\frac{RMS_v812}{RMS_v258B}$	$\frac{RMS_CFD950}{RMS_v258B}$
47	0.304303	0.487637
105	0.653006	0.533675
202	0.879654	0.689716
298	0.808959	0.722029

Table 3: Constant fraction discriminator time resolution to fixed threshold discriminator time resolution at various input amplitudes with 10mV sinusoidal modulation.

Although v812 outperforms CFD950 at small input amplitudes of 47mV, averaging across the 4 different input amplitudes gave $\frac{RMS_v812}{RMS_v258B} = (0.7 \pm 0.3)$ and $\frac{RMS_CFD950}{RMS_v258B} = (0.6 \pm 0.1)$. However, a typical MIP signal has amplitude of 23mV and extrapolation from the data in table 3 suggests that v812 might be a better choice for signals with small amplitudes.

The improvement of the constant fraction discriminator time resolution is dependent on input amplitude, with the improvement most significant for small input signals with ampli-

tudes around 50mV. Large signals (amplitudes $\sim 2V$) are more resilient to noise (sinusoidal modulation with 10mV amplitude) and the fixed threshold discriminator is able to discriminate the signals even in the presence of noise. This diminishes the significance of the time resolution improvement observed in the constant fraction discriminators.

3.2.2 Summing across all input amplitudes

The time resolution for the fixed threshold discriminator (v258B) is the poorest due to time walk, as manifested in the shifting of the histogram of discriminator output arrival times in figure 6. The histograms in figure 7 were not fitted with any distributions as the original measurements, shown in figure 6, were not taken at regular intervals of input amplitude. This lack of contribution from certain input amplitudes will result in asymmetry, as seen in the histogram for v258B in figure 7.

The histogram of discriminator output arrival times for v812 has the smallest RMS, followed by the histogram corresponding to CFD950 and finally v258B. Taking ratio of the histogram RMS of the constant fraction discriminators to the fixed threshold discriminator gave $\frac{RMS_v812}{RMS_v258B} = (0.1 \pm 0.1)$ and $\frac{RMS_CFD950}{RMS_v258B} = (0.1 \pm 0.1)$. This suggests that the constant fraction discriminators (v812, CFD950) have better time resolutions 10 times better than that of the fixed threshold discriminator (v258B).

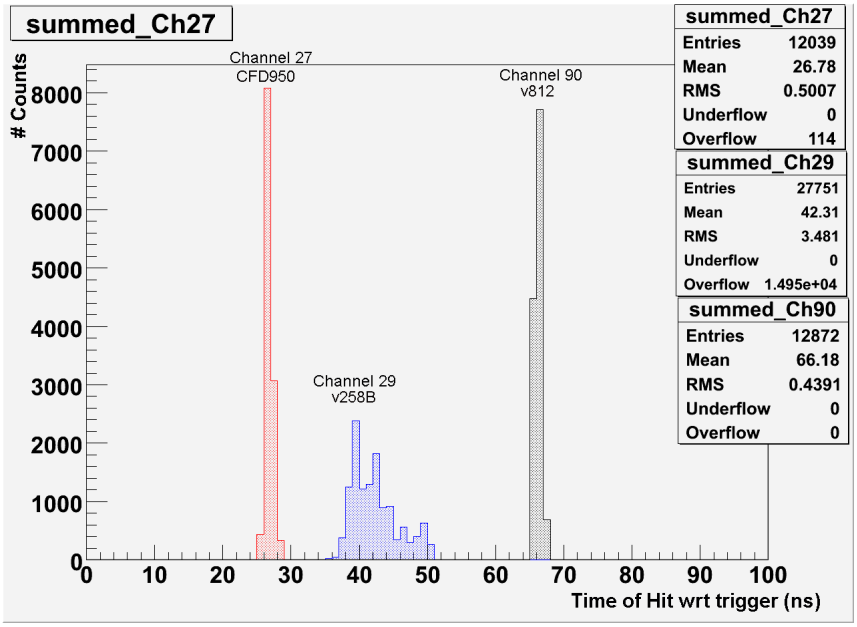

Figure 7: Summing up histograms for each discriminator across all input amplitude for threshold of -20mV, 10mV sinusoidal modulation amplitude.

The overflow entries of the histogram corresponding to v258B might have been recorded when the discriminator fails to accurately discriminate an incoming signal, giving an output pulse which arrives at the TDC at a time that varies greatly different from the rest output signals. Significantly more overflow entries were observed for v258B (1.495e4 overflow entries) than that for CFD950 (114 overflow entries), while no overflow entries were

observed for v812. This suggests that v812 might be more robust against input signals with fluctuating amplitudes.

4 Conclusions

Testing the various discriminators with generic pulses yield promising outcomes, with both constant fraction discriminators (v812, CFD950) showing clear improvements in time resolution. Considering signals with input amplitudes of approximately 50mV subjected to sinusoidal modulations of 10mV, v812 improved the time resolution by slightly more than a factor of 3 while CFD950 improved time resolution by approximately a factor of 2. However, CFD950 has a shorter dead time of (11.0±0.3)ns for input pulses with widths less than 50ns while the of the dead time of v812 is yet to be understood thoroughly.

Acknowledgements

I would like to thank my supervisors Wolfgang Lohmann, Elena Castro and Olga Novgorodova for their patient and meticulous guidance. I would also like to extend my appreciation to Wolfgang Lange and Hans Henschel, for their invaluable advice on hardware and instrumentation that could only be gathered via experience. Lastly, I would like to thank DESY for giving me this oppportunity to participate in this Summer Student Programme.

References

[1] Lyndon Evans and Philip Bryant. Lhc machine. *Journal of Instrumentation*, 3(08):S08001, 2008.

[2] The CMS Collaboration, S Chatrchyan, G Hmayakyan, V Khachatryan, A M Sirunyan, W Adam, T Bauer, T Bergauer, H Bergauer, M Dragicevic, J Erö, M Friedl, R Frühwirth, V M Ghete, P Glaser, C Hartl, N Hoermann, J Avezov, M I Fazylov, E M Gasanov, A Khugaev, Y N Koblik, M Nishonov, K Olimov, A Umaraliev, and B S Yuldashev. The cms experiment at the cern lhc. *Journal of Instrumentation*, 3(08):S08004, 2008.

[3] A. Bell, E. Castro, R. Hall-Wilton, W. Lange, W. Lohmann, A. MacPherson, M. Ohlerich, N. Rodriguez, V. Ryjov, R. S. Schmidt, and R. L. Stone. Fast beam conditions monitor BCM1F for the CMS experiment. *Nuclear Instruments and Methods in Physics Research A*, 614:433–438, March 2010.

[4] M. Beuzekom. *Identifying fast hadrons with silicon detectors*. PhD thesis, University of Groningen Faculty of Mathematics and Natural Sciences Dissertation, 2006.

[5] Helmuth Spieler. *Semiconductor Detector Systems*. Oxford University Press, first edition, 2005.